Journal of Constructional Steel Research 106 (2015) 311–321

Contents lists available at ScienceDirect

Journal of Constructional Steel Research

Development of a buckling restrained shear panel damper

Kailai Deng [a], Peng Pan [b,*], Wei Li [a], Yantao Xue [c]

[a] Department of Civil Engineering, Tsinghua University, Beijing 100084, China
[b] Key Laboratory of Civil Engineering Safety and Durability of China Education Ministry, Department of Civil Engineering, Tsinghua University, Beijing 100084, China
[c] Institute of Building Structures, China Academy of Building Research, Beijing 100013, China

ARTICLE INFO

Article history:
Received 17 June 2014
Accepted 6 January 2015
Available online 19 January 2015

Keywords:
Buckling restrained shear panel damper
Low cycle fatigue
Quasi-static test
Numerical analyses
Design method

ABSTRACT

Steel shear panel dampers (SPDs) have been widely used in structural seismic design. The low cycle fatigue damage for SPD often occurs close to the welded stiffener, significantly weakening the fatigue performance of the damper. A novel steel shear panel damper called a buckling restrained shear panel damper (BRSPD) is proposed in this paper. A BRSPD has two main parts, an energy dissipation plate and two restraining plates. No stiffener is welded to the energy dissipation plate. The two restraining plates clamp the energy dissipation plate with bolts on both sides to prevent out-of-plane buckling. Quasi-static tests of five specimens were carried out to investigate the performance of the BRSPDs. The test focused on the stiffness and strength of the restraining plates and the gaps between them and the energy dissipation plate. The tests showed that the restraining plates with adequate stiffness and strength can effectively restrain the out-of-plane buckling of the energy dissipation plate. Numerical analysis of the BRSPD was conducted using the general finite element program, ABAQUS, to supplement the test results. A design method for the restraining plates and the bolts is suggested based on the test and analysis results.

1. Introduction

Shear panel dampers (SPDs) are widely used in the seismic design of structures because of their low cost and stable energy dissipation capacity [1–7]. The typical installation of SPD in a frame structure is shown in Fig. 1. The SPD sustained large shear deformation and dissipated energy in earthquakes. Considerable research has been carried out to improve the low cycle fatigue performance of the SPD. This research has focused on the effects of steel materials and the arrangement of the stiffeners of the SPD. Nakashima et al. investigated the performance of SPDs made of low-yield steel [8,9]. It was observed that SPDs using low yield steel have a better low cycle fatigue performance under cyclic loading than those using ordinary steel. Currently most SPDs used in practical engineering are made of low-yield steel or aluminum alloy, which has excellent deformation capacity [10–14]. Ohsaki et al. optimized the arrangement of the stiffener to maximize the energy dissipation capacity of the SPD [15]. The simulated annealing algorithm was adopted in this nonlinear structural optimization problem. The results showed that with the optimal arrangement of the stiffener the maximum equivalent plastic strain (EPS) of the SPD under cyclic loading was significantly reduced and the low cycle fatigue performance of the SPD was much improved. Zhang et al. carried out a series of tests on the SPD with different shapes of the energy dissipation plate [16,17]. To avoid low cycle fatigue damage at the heated affected zone of the weld, the central area of the energy dissipation plate was intentionally weakened. The results showed that the low cycle fatigue behavior of the SPD with a weakened energy dissipation plate was better than that of the conventional one.

The low cycle fatigue damage was likely to occur at the heat affected zone of the weld for the conventional SPD when it was subjected to cyclic loading. The weld significantly decreased the fatigue strength of the steel [18–20]. Some research was carried out to improve the low cycle fatigue performance of the SPD by removing the welded stiffeners. However, the stress distribution of the energy dissipation plate without stiffeners changed significantly, and the plastic strain was concentrated at the corner of the plate, which was harmful for the low cycle fatigue performance of the SPD [21]. To avoid plastic strain concentration, Liu et al. conducted several tests to obtain the strain distribution of SPDs with different shapes under cyclic loading [22]. They also built a finite element model using ABAQUS and conducted shape optimization of the energy dissipation plate. The edge of the SPD was assumed to be parabolic and the optimal parameters for the parabola were obtained using regression analysis. With the optimal shape the maximum EPS values were significantly less. Deng et al. adopted a simulated annealing algorithm for the shape optimization of the energy dissipation plate [23]. The optimal shape obtained in this study provided a more uniformly distributed EPS according to the elastic–plastic analysis results using ABAQUS. The maximum EPS of the SPD with an optimally shaped web was only about one-third of the EPS for the SPD with a conventional rectangular energy dissipation plate. However, out-of-plane buckling may occur when the SPD sustains a large shear deformation. Brando et al. proposed a hysteretic damper, whose main energy

* Corresponding author. Tel.: +86 10 62794729; fax: +86 10 62788620.
E-mail address: panpeng@mail.tsinghua.edu.cn (P. Pan).

http://dx.doi.org/10.1016/j.jcsr.2015.01.004
0143-974X/

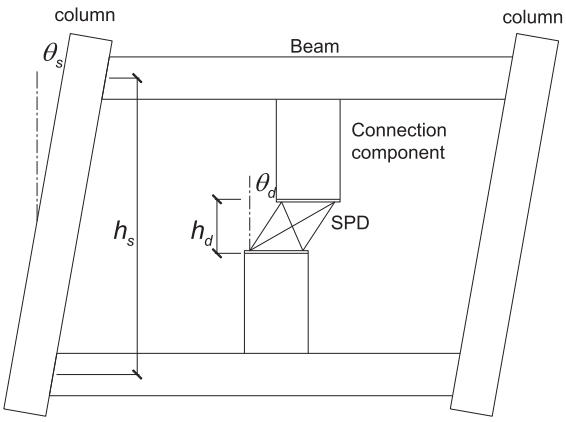

Fig. 1. Installation of SSPD.

dissipation part is made of aluminum alloy [24]. The aluminum alloy plate sustains shear deformation and dissipates energy through plastic deformation. The out-of-plane deformation of the aluminum plate is inhibited by two steel plates. The experiment proved that the inhibiting mechanism enhanced the performance of the hysteretic damper compared to the damper without the restraining plate.

A novel SPD called a buckling restrained shear panel damper (BRSPD) is proposed in this study. The BRSPD contains two parts, an energy dissipation plate and two external restraining plates. The two restraining plates clamp the energy dissipation plate with bolts on both sides to prevent out-of-plane buckling. Quasi-static tests were carried out to investigate the mechanical performance of the BRSPD under cyclic loading. In total four BRSPD specimens were tested by taking the stiffness and strength of the external restraining plates and the width of the gaps between the energy dissipation plate and the external restraining plates as the major test parameters. Finite element analyses were conducted to supplement the physical test results, and formula to estimate the BRSPD strength was proposed based on the test and analysis results. Finally the stiffness demands of the external restraining plates were derived based on the buckling analysis of the plates.

2. Buckling restrained shear panel damper

As shown in Fig. 2, the BRSPD consists of two parts, an energy dissipation plate and two external restraining plates. The energy dissipation plate was welded on both the upper and lower connection plates, and it sustained shear deformation and dissipated energy during earthquakes. To avoid concentration of the plastic strain the optimal shape of the energy dissipation plate, obtained from reference [23], was adopted in this study.

External restraining plates were installed on each side of the energy dissipation plate. The gaps between the energy dissipation plate and the external restraining plates should be accurately controlled. As shown in Fig. 2, a gasket is installed between the two external restraining plates to control the gap's size. When the energy dissipation plate buckles under cyclic loading, it will make contact with the external restraining plates. The bolts are used to bind the two external restraining plates, so that they can clamp the energy dissipation plate and prevent it from out-of-plane deformation. With the external restraining plates, the energy dissipation plate can provide a stable restoring force when subjected to cyclic shear deformation.

As shown in Fig. 2(d), the external restraining plates were welded to the lower connection plate at each end. A cut was configured at the bottom of the external restraining plates to leave a space for the fillet weld

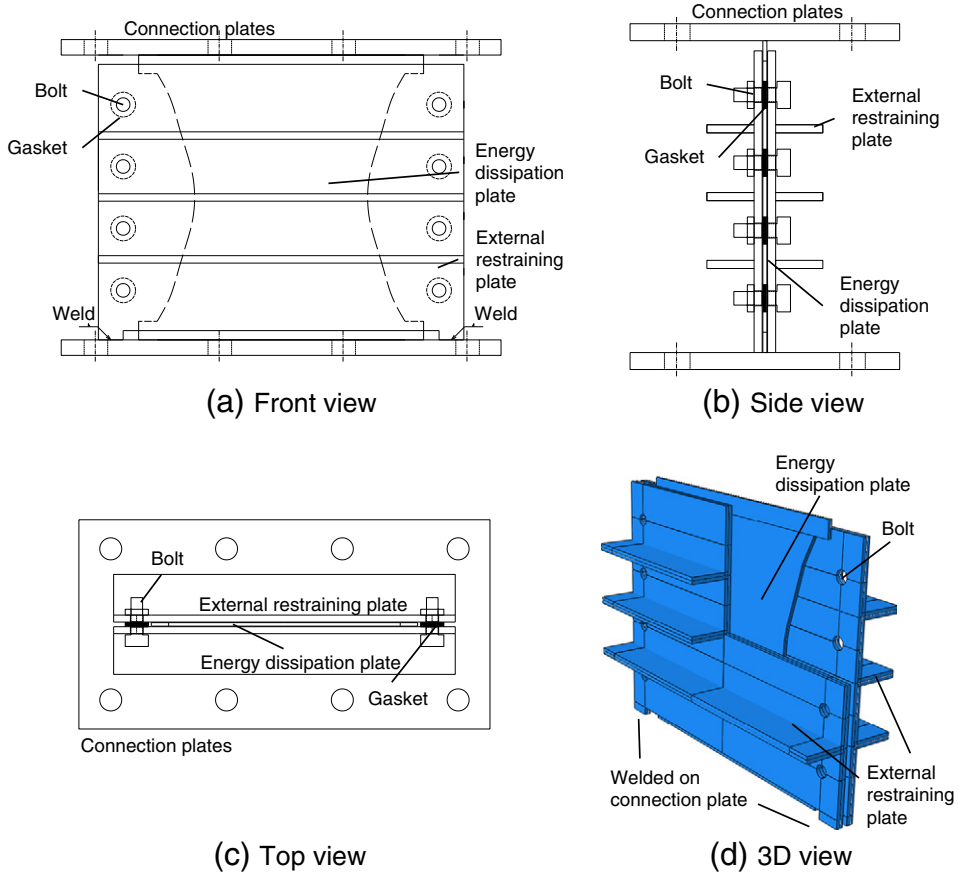

Fig. 2. Structure of the BRSPD.

of the energy dissipation plate. The external restraining plates were welded to the lower connection plate but not connected to the upper connection plate. With such a structure, the external restraining plates did not provide any restoring force. The external restraining plates should have sufficient stiffness to provide the restraining effect. To effectively restrain the out-of-plane deformation of the energy dissipation plate, the gaps between the external restraining plates and the energy dissipation plate should not be too large.

3. Experimental study

3.1. Test plan

As shown in Table 1, five specimens, designated S1 to S5, were designed to investigate the performance of the BRSPD under cyclic loading. The energy dissipation plates for S1 to S5 were identical and were made of LY225, which have proved to have a satisfactory low cycle fatigue property [25,26]. As shown in Table 2, the yield stress and the ultimate stress of LY225 are 233 MPa and 333 MPa, respectively. The energy dissipation plate was 6-mm-thick, and details of the dimensions are given in Fig. 3(a). The core energy dissipation zone lies between the two spline edges. The width and the height of the core energy dissipation zone were both 400 mm. A fillet weld with 6 mm thickness was adopted to connect the energy dissipation plate to the upper and lower connection plates. At the top and the bottom of the energy dissipation plate, two areas 30 mm wide were configured as the heat affected zones of the welds. The steel plate in the heat affected zones of the welds did not yield. The external restraining plate is made of Q235B, which has a yielding stress of 290 MPa and an ultimate stress of 479 MPa. Note that the nominal strength of Q235B is 235 MPa in Chinese steel design code. The size of the gaps between the external restraining plates and the energy dissipation plate, and the stiffness of the external restraining plates, were taken as the major test parameters in this study. S1 is the standard specimen with a gap of 1 mm, which uses an 8-mm-thick gasket to control the gap's size between the two external restraining plates. The thickness of the external restraining plates was 12 mm, and 3 horizontal stiffeners were welded to the external restraining plate to enhance its bending stiffness [Fig. 3(b)].

The external restraining plates are weld to the lower connection plate. The fillet weld on the external restraining plates is 8 mm. High strength bolts with a diameter of 10 mm are used to connect the two external restraining plates. S2 and S3 were used to study the restraining effect, while S4 and S5 were used to investigate the width of the gaps between the energy dissipation plate and the external restraining plates. S2 did not have any external restraining plates. The external restraining plates for S3 were steel plates 6 mm thick with no stiffeners welded to it. S4 has a gap of 2 mm, twice as large as that of S1, which uses a 10-mm-thick gasket. No gaps were set between the energy dissipation plate and external restraining plates for S5. No gasket was equipped in S5.

As shown in Fig. 1, h_s, θ_s, h_d, and θ_d are the story height, story drift, damper height and shear deformation angle of damper. Eq. (1) indicates the relationship between story drift and shear deformation angle of damper. In Chinese engineering practice, the story drift is usually designed about 1/100 under maximum consider earthquake, and the ratio of story height to damper height is about 6. Assuming that the connection component is rigid, the shear deformation angle of the damper is 1/17. Considering the deformation of the connection component, the maximum deformation angle of the BRSPD is set to 1/20.

$$\theta_d = \frac{h_s}{h_d}\theta_s \tag{1}$$

The loading history is shown in Fig. 4. The BRSPDs were first loaded at amplitudes of 5 mm and 10 mm, and each amplitude was loaded for three cycles. The BRSPDs were then loaded to an amplitude of 20 mm for multiple cycles until failure occurred. The amplitude of 20 mm corresponded to a shear angle of 1/20. The loading setup is shown in Fig. 5. Totally 8 high-strength anchor bolts are used to tie the loading frame to the ground. Each anchor bolt has a diameter of 80 mm. The cross section of the two vertical steel components is shown on the right side of Fig. 5. Each of the vertical steel components has an area of 45,200 mm^2, ensuring adequate stiffness of the loading frame. The upper and lower connection plates of the BRSPD were bolted to the loading frame using high strength bolts. The frame had four pin connections, which could rotate freely. The forces exerted by the actuator were considered equal to the restoring forces provided by the BRSPDs. A displacement transducer was installed between the upper and lower connection plates to control the shear deformation of the BRSPD. The control accuracies of the force sensors and the displacement transducers are 0.25 kN and 0.01 mm respectively.

Table 2
Mechanical features of the steel.

Steel type	Yield stress (MPa)	Ultimate stress (MPs)	Stiffness (GPa)
LY225	233	333	201
Q235B (6 mm)	293	482	207
Q235B (12 mm)	287	475	207

3.2. Test results

The hysteresis curve for S1 is shown in Fig. 6(a). It was stable and saturated, demonstrating the satisfactory energy dissipation capacity of the BRSPD. The maximum restoring force for S1 was about 308 kN. Although the peak restoring force does not decrease, an obvious pinching effect can be observed on the hysteresis curve for the first 10 loading cycles at 20 mm amplitude. This phenomenon is induced by the buckling of the energy dissipation plate. For S1, the external restraining plates do not “perfectly” restrain the buckling deformation of the energy dissipation plate, because the 1-mm-wide gaps give the energy dissipation plate spaces to have tension field action. An obvious degradation of the peak restoring force occurred at the 10th cycle of loading at an amplitude of 20 mm, which may induced by the low cycle fatigue damage of the energy dissipation plate. At the 16th cycle of loading at an amplitude of 20 mm, the restoring force decreased to 85% of the peak value, indicating a failure of the damper according to the criteria prescribed in the seismic design code [27]. Fig. 6(b) presents the ultimate failure mode of the energy dissipation plate for S1. Low cycle fatigue damage occurred at the free edge of the energy dissipation plate, which agreed with the results predicted in reference [23]. Note that the external restraining plate for S1 had no visible deformation during the test.

Table 1
Details for the five specimens.

Specimen	Size of gap (mm)	Restraining plate	Remarks
S1	1	12 mm thick plate with 3 stiffeners	Standard specimen
S2	N/A	N/A	No restraining plate
S3	1	6 mm thick plate without stiffeners	Weak restraining plate
S4	2	12 mm thick plate with 3 stiffeners	Large gap
S5	0	12 mm thick plate with 3 stiffeners	No gap

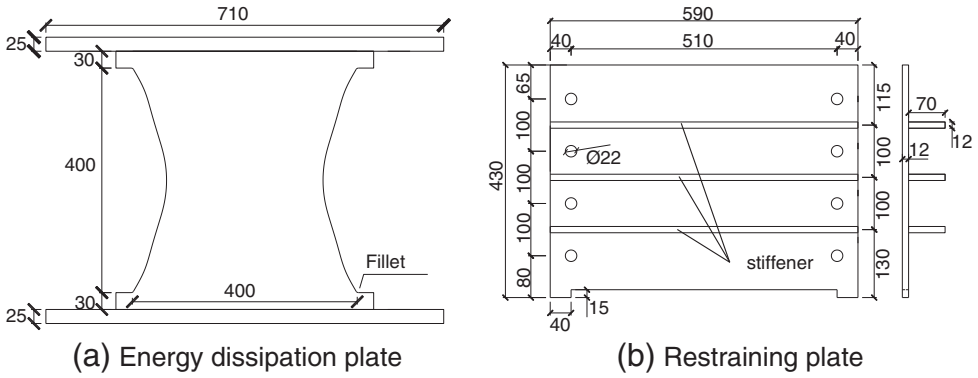

Fig. 3. Detailed dimension of a specimen (mm).

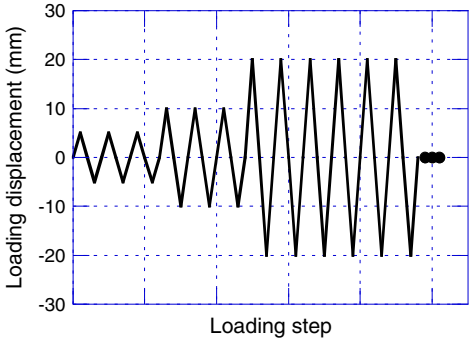

Fig. 4. Loading history.

The hysteresis curve for S2 is presented in Fig. 6(c). The restoring force for S2 decreased from the 1st cycle of loading at an amplitude of 5 mm. as shown in Fig. 6(d). Significant out-of-plane buckling of the energy dissipation plate was observed, creating a significant pinching effect on the hysteresis curve. This was because S2 did not have any external restraining plates, and its energy dissipation plate got buckled very early. The maximum restoring force was about 200 kN. After three cycles of loading at an amplitude of 20 mm, the restoring force decreased to about 160 kN.

The external restraining plates for S3 had no stiffener, and were 6 mm thick. As shown in Fig. 6(e), S3 has a similar hysteresis curve to S2. The hysteresis curve for S3 was slightly more saturated than that for S2. After 4 cycles of loading, the restoring force decreased to 85% of the peak value, indicating unsatisfactory low cycle fatigue behavior. The failure mode for S3 is shown in Fig. 6(f). The external restraining plates deformed, and the energy dissipation plate buckled seriously. The weak external restraining plates could not effectively restrain the out-of-plane deformation of the energy dissipation plate. It should be noted that the out-of-plane buckling pattern for S2 and for S3 were quite different. As shown in Fig. 6(d), S2 presented an overall torsional deformation, while, because of the inadequate restraining effect in S3, the central area of the energy dissipation plate bulged outward. The external restraining plates could be taken as a simply supported beam along the horizontal direction. The central area of the plates was prone to bending.

S4 had 2 mm gaps between the external restraining plates and the energy dissipation plate. The hysteresis curve for S4 is shown in Fig. 6(g). It was similar to that for S1 and was stable and saturated. However, the post-yield stiffness for S4 presented more notable degradation in each cycle of loading from the 2nd to the 4th cycle. The too wide gaps between the energy dissipation plate and external restraining plates left too much space for the out-of-plane deformation of the energy dissipation plate. The maximum restoring force for S4 was about 308 kN, and decreased to 85% of the peak value at the 10th cycle of loading at an amplitude of 20 mm. The ultimate failure pattern of the energy dissipation plate was similar to that for S1, namely, low cycle fatigue damage appeared on the spline edge.

No gap was configured between the external restraining plates and the energy dissipation plate for S5. The hysteresis curve for S5 is presented in Fig. 6(h), and was more stable than that for S1. The maximum restoring force for S5 was about 317 kN. Due to no gap left, the punching

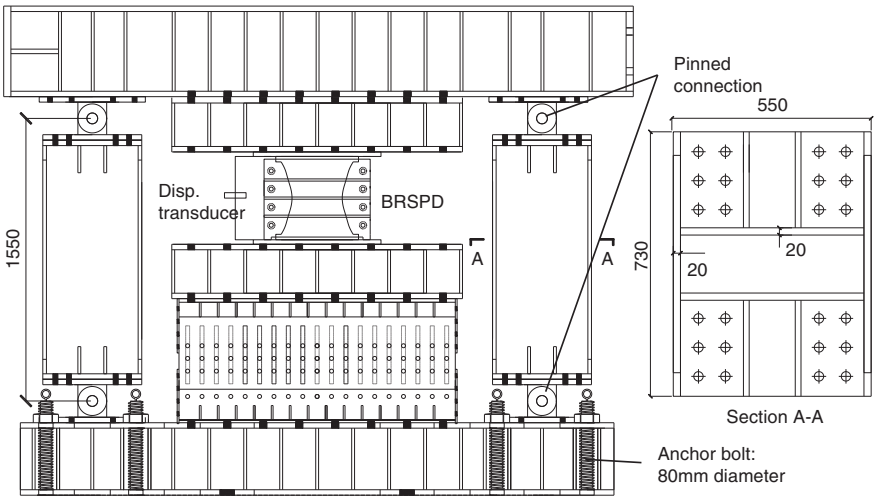

Fig. 5. Test setup.

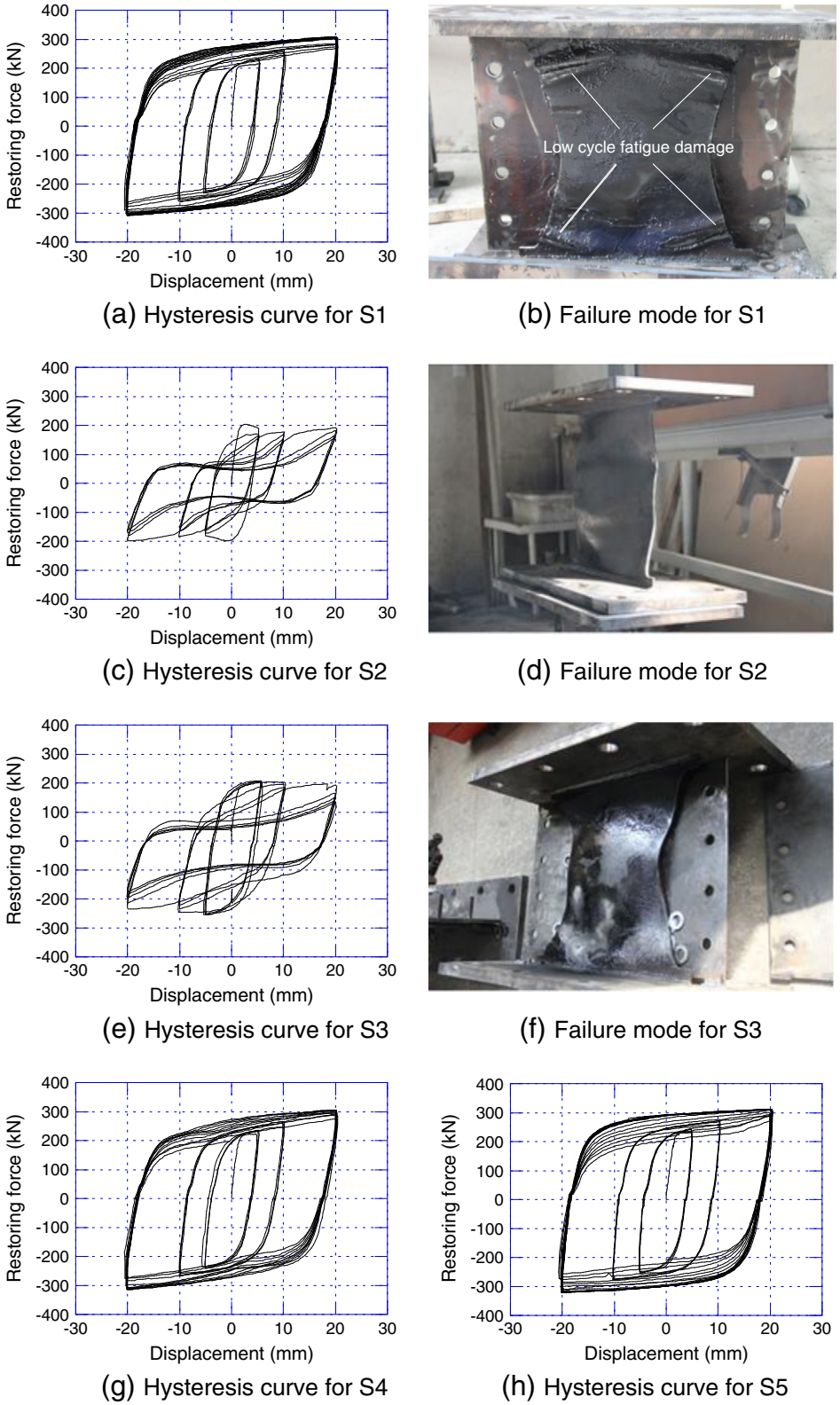

Fig. 6. Test results.

effect of S5 is slighter than S1 in the beginning of 1/20 deformation angle loading. Similar to S1, S5 was damaged at the 16th cycle of loading at an amplitude of 20 mm. The failure of S5 was caused by the low cycle fatigue damage on the free edge, which was identical to that of S1. Based on the results for S5, it was concluded that the configuration of the gaps between the core energy dissipation unit and outer restraining units for the BRSPD was different to that of the buckling restrained braces (BRB). Note that generally BRB required adequate gaps between the core energy dissipation unit and outer restraining units.

According to the test, S1 and S5 performed better than others in terms of low cycle fatigue behavior. It was concluded that the external restraining plates should have sufficient stiffness and strength and the

gaps between external restraining plates and energy dissipation plate should be no more than 1 mm.

4. Numerical analysis

4.1. Numerical model

Finite element analyses were conducted to further investigate the performance of the BRSPD. As shown in Fig. 7, the numerical model of the BRSPD was created in ABAQUS. The S4R element, which was a 4-node general-purpose shell that reduced the integration with hourglass control and finite membrane strains, was adopted to simulate the energy dissipation plate and external restraining plates. Reference [23] conducted a sensitive analysis on the mesh size for the shape optimization of the energy dissipation plate. The mesh size used in this study is about 10 mm, which is identical with that recommended in reference [23]. ABAQUS provided a numerical material law for metals subjected to cyclic loading. The kinematic hardening stress is described as Eq. (2), in which C_k and γ_k are the coefficients. As shown in Table 3, the parameters used in this paper are determined in reference to the previous studies presented in [28,29].

$$\alpha = \sum_{k=1}^{n} \frac{C_k}{\gamma_k}\left(1 - e^{-\gamma_k \bar{\varepsilon}^{pl}}\right) \tag{2}$$

The contact between the energy dissipation plate and the external restraining plates were modeled as “hard contacts”. The constitutive model of a “hard contact” is shown in Fig. 8. Normal contact pressure is generated when the two surfaces touch, whereas no pressure exists when they separate. Coulomb friction was employed to simulate the behavior between the contacted surfaces in the tangential direction. The friction coefficient was 0.3 in this study. The edge of the bolt hole on the external restraining plates was constrained to the respective reference point. Two corresponding reference points were connected by a spring element, which had the same stiffness as the bolt. The out-of-plane performance was sensitive to the initial imperfection of the plates. Buckling analysis was conducted first. Fig. 9 shows the 1st order buckling mode of an energy dissipation plate. For the energy dissipation plate, the even-order buckling modes are anti-symmetric to the corresponding odd-order buckling modes, and no imperfection can be applied if the first two buckling modes with identical magnitudes are considered simultaneously. In addition, the higher order buckling modes, e.g. 3rd, 5th, and 7th, have little effects on the results of the numerical analyses. Therefore, only the 1st buckling mode is considered for the initial imperfection. The maximum magnitude of the initial imperfection was 0.5 mm, following the suggestion given in the Code for

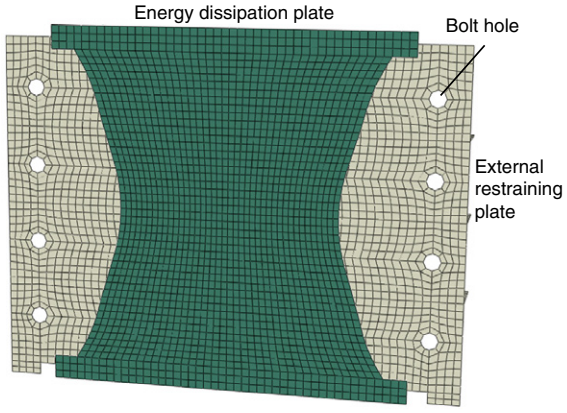

Fig. 7. Numerical model of ABAQUS.

Table 3
Parameters for the numerical material law (MPa).

σ_0	C_1	γ_1	C_2	γ_2	C_3	γ_3	C_4	γ_4
185	22,000	300	1600	120	6000	250	600	30

the design of steel structures [27]. The loading history was the same as that adopted in the physical test.

Fig. 10 compares the results of the finite element analyses and those of the physical tests. As shown in Fig. 10(f), the ultimate failure pattern for S3 obtained from the numerical analysis was similar to that obtained from the physical test, demonstrating the effectiveness of the model for simulating the restraining mechanism. The hysteresis curves obtained from numerical models precisely fit those obtained from the physical tests for the specimens with satisfactory restraining effects, whereas discrepancies are notable for the specimens not well restrained. The energy dissipation plate buckles if it is not well restrained, and the buckling behavior is sensitive to many factors, e.g. initial imperfection, post-yield behavior of material, and mesh size. Precisely simulating the buckling behavior is interesting and challenging, but it is not the focus of this paper.

It should be noticed that the restoring force for S5 obtained from the physical test was slightly larger than the value obtained from the numerical analysis. A pre-tension force existed in the bolts of S5 in the physical test, while it was not considered in the numerical analysis. The pre-tension force induced additional friction, leading to a larger restoring force for S5 in the physical test. Furthermore, the numerical material model did not consider the low cycle fatigue damage, so that the decrease in the restoring caused by fatigue damage would not be simulated in the finite element analysis results.

Fig. 11(a) presents the contact stress distribution of the external restraining plate. It can be observed that the contact area was in a diagonal direction, which agreed with the buckling mode of the conventional steel shear panel.

The tensile forces on the bolts obtained from the numerical models for S1, S4 and S5 are presented in Fig. 11(b). The bolt forces increased with the loading cycles. Within 20 cycles of loading at an amplitude of 20 mm, the maximum total bolt forces for S1, S4 and S5 were 151.33 kN, 207.34 kN and 68.11 kN, respectively. For each BRSPD, the forces sustained by the eight bolts were different. The bolts in the middle had the largest bolt forces, which were 45.2 kN, 46.04 kN and 33.52 kN for S1, S4 and S5, respectively. This was because the energy dissipation plate had the largest deformation in the middle, and the larger out-of-plane deformation led to greater contact pressure.

4.2. Parametric analysis

Because the number of test specimens was limited, more finite element analyses were carried out to quantitatively investigate the restoring force for the BRSPD. The parametric analysis focuses on the specimens with satisfactory restraining. As discussed above, the numerical model has satisfactory precision for the BRSPD with reliable restraint. Fifteen supplementary models with different energy dissipation plates were built. The main parameters were the width and height of the plates. The details of the supplementary models are given in Table 4. The gaps between the energy dissipation plate and the external restraining plates were 1 mm for all the supplementary models. The loading history for the supplementary analyses was the same as those adopted in the physical tests.

Fig. 12(a) presents relationship between the initial stiffness and the width of the energy dissipation plate for the 15 supplementary models. Fig. 12(b) presents relationship between the energy dissipation capacity and the width of the energy dissipation plate. The dissipated energy in Fig. 12(b) is defined as the area of the 1st loop on the hysteresis curve for the 20 mm amplitude. In both figures, the results are plotted for the energy dissipation plates with different heights separately. It can

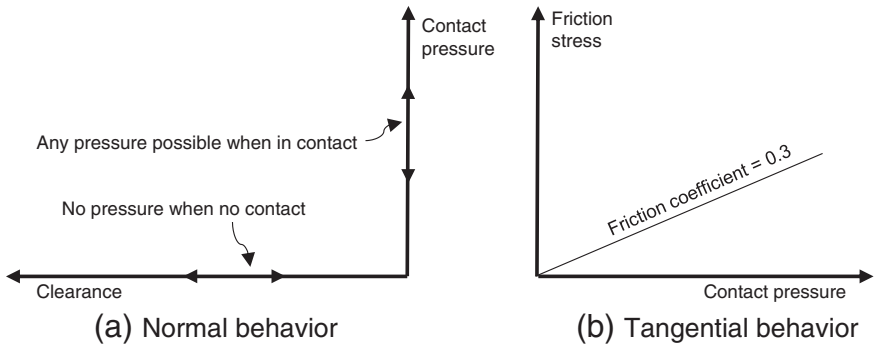

Fig. 8. Constitutive model of "hard contact".

be observed that a wider energy dissipation plate leads to larger stiffness and energy dissipation capacity, and a taller energy dissipation plate induces smaller stiffness and energy dissipation capacity. Furthermore, both the stiffness and the energy dissipation capacity present strong linear correlation to the width of the energy dissipation plate with a correlation coefficient more than 0.99.

The ultimate restoring force is important for calculating the stiffness demand of the external restraining plate. The ultimate restoring force for the 15 BRSPDs is presented in Fig. 13(a). The relationship between ultimate restoring force to the height and width of energy dissipation plate is similar with the stiffness. For the BRSPDs with the same width, the taller energy dissipation plate had a relatively larger cutting profile for the optimal shape. Thus, the BRSPD with the taller energy dissipation plate provided a relatively smaller restoring force. Linear correlation coefficients are also presented in Fig. 13(a), which were no less than 0.9990, demonstrating a strong linear relationship between the restoring force and the width of the energy dissipation plate. Based on the results obtained from the parametric analyses, the ultimate restoring force for the BRSPD can be calculated using Eq. (3):

$$F_u = \left(\frac{\alpha}{h^{\beta}}\right)\frac{f_u bt}{\sqrt{3}}, \tag{3}$$

where, $f_u/\sqrt{3}$ is the ultimate shear strength of the steel, which was 179.3 MPa in this study. b and t are the width and thickness of the energy dissipation plate. Thus, $f_u bt$ indicates the ultimate shear strength of the rectangular energy dissipation plate without cutting, while α/h^{β} indicates the reduction in strength caused by the shape optimization. α and β are the fitting parameters. The least squares method was adopted when determining the fitting parameters. The parameters in this study were $\alpha = 14.17$ and $\beta = 0.4901$. Note that the units in Eq. (3) should be "mm" and "MPa".

Another two models are built to validate the effectiveness of Eq. (3). The dimensions of the energy dissipation plates are $360 * 450$ mm^2 and $450 * 495$ mm^2 for the two models, respectively. Fig. 13(b) compares the ultimate restoring forces obtained from the numerical analysis and those predicted by Eq. (3). According to Fig. 13(b), the maximum relative error is no more than 4%, demonstrating the effectiveness of Eq. (3). Thus, Eq. (3) can be used to estimate the stiffness demand of the external restraining plate.

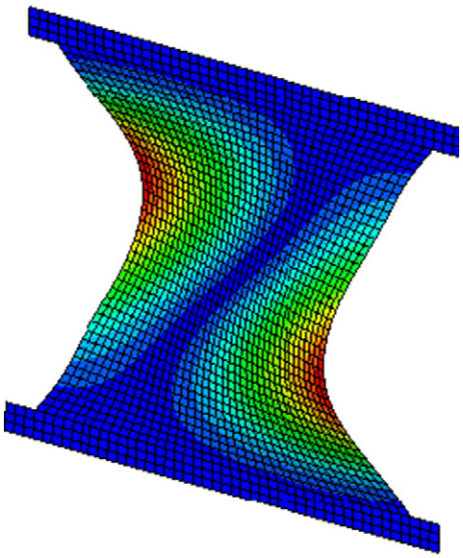

Fig. 9. 1st order buckling mode.

5. Stiffness demand of the external restraining plate

The critical buckling force for the energy dissipation plate was calculated using Eq. (4) [30]. D_e is the bending stiffness of the energy dissipation plate, equal to $Et^3/12(1-\nu^2)$. E and ν are the elastic module and Poisson's ratio of steel. k_{cr} is the elastic buckling coefficient. Because of the irregular shape of the energy dissipation plate, the analytical expression of k_{cr} was difficult to derive. A simple approach to obtaining the buckling coefficient is regression analysis. Buckling analyses on 15 supplementary models were carried out in ABAQUS, and the buckling coefficients for the 15 models were obtained. A simple quadratic polynomial, shown in Eq. (5), was adopted to express the buckling coefficient in the regression analysis. Fig. 14 compares the elastic buckling coefficient k_{cr} obtained from the finite element buckling analyses and Eq. (5). The error was no more than 8%, and the correlation coefficient was 0.9959, demonstrating the effectiveness of the regression analysis.

$$F_{cr} = k_{cr}\frac{\pi^2 D_e}{b} \tag{4}$$

$$k_{cr} = 4.934\left(\frac{b}{h}\right)^2 + 0.5646\left(\frac{b}{h}\right) - 1.507 \tag{5}$$

The equilibrium differential equations for the energy dissipation plate and external restraining plates are given in Eqs. (6) and (7) [30], where ω is the out-of-plane deflection of the energy dissipation plate and D_r is the bending stiffness of the external restraining plate. Note that Eqs. (6) and (7) assume that the energy dissipation plate and the external restraining plates have the same out-of-plane deformation.

$$-D_e\left(\frac{\partial^4\omega}{\partial x^4} + 2\frac{\partial^4\omega}{\partial x^2\partial y^2} + \frac{\partial^4\omega}{\partial y^4}\right) + N_y\frac{\partial^2\omega}{\partial y^2} + 2N_{xy}\frac{\partial^2\omega}{\partial x\partial y} = -p(x,y) \tag{6}$$

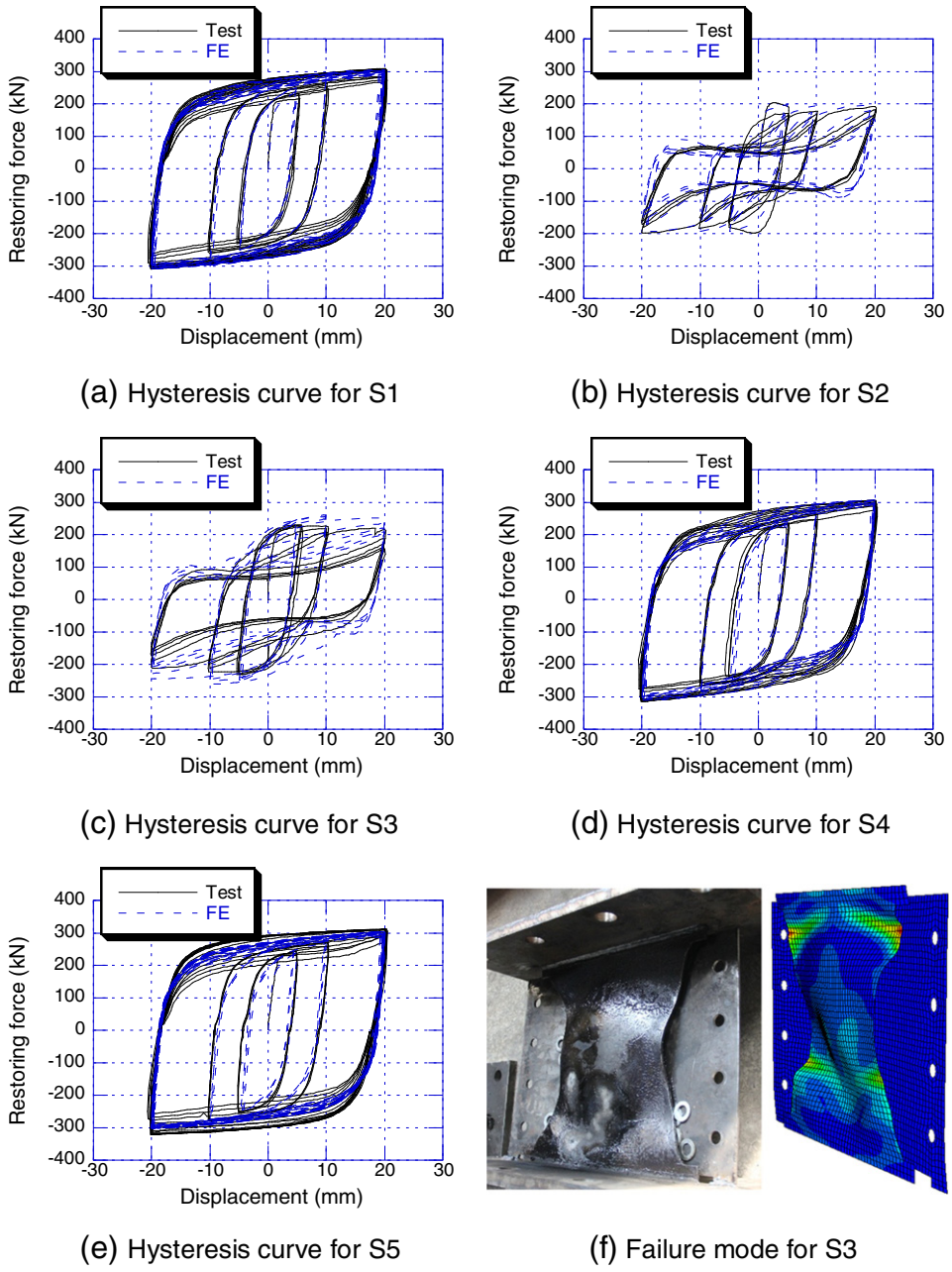

Fig. 10. Comparison between the numerical analyses and physical tests.

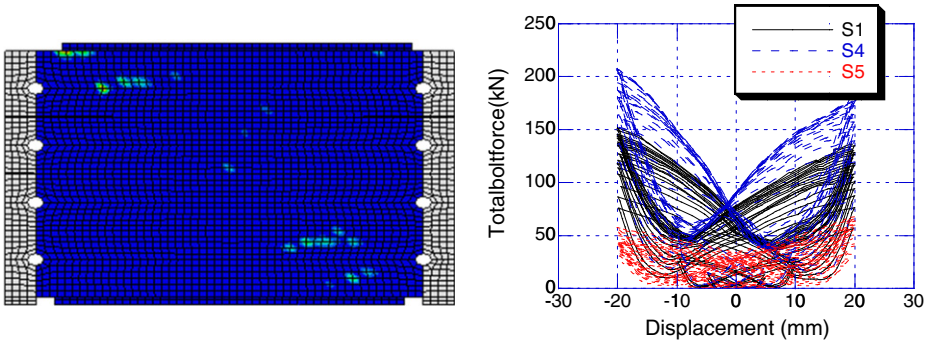

Fig. 11. Contact stress and total bolt force.

Table 4
Parameters for the supplementary models.

Width (mm)	Height (mm)	Total
400, 450, 500, 550, 600	300, 400, 500	15

$$-D_r\left(\frac{\partial^4\omega}{\partial x^4}+2\frac{\partial^4\omega}{\partial x^2\partial y^2}+\frac{\partial^4\omega}{\partial y^4}\right)=p(x,y) \tag{7}$$

N_y and N_{xy} are the normal stress and shear stress on the clamped edge of the energy dissipation plate, expressed by Eqs. (8) and (9). F_u is the ultimate restoring force, calculated using Eq. (3). $p(x,y)$ is the contact force.

$$N_y=\frac{3F_u b(b-2x)}{b^3} \tag{8}$$

$$N_{xy}=\frac{6F_u(b-x)x}{b^3} \tag{9}$$

The equilibrium differential equation for the energy dissipation plate and the external plates can be derived by solving Eqs. (6) and (7).

$$-(D_e+D_r)\left(\frac{\partial^4\omega}{\partial x^4}+2\frac{\partial^4\omega}{\partial x^2\partial y^2}+\frac{\partial^4\omega}{\partial y^4}\right)+N_y\frac{\partial^2\omega}{\partial y^2}+2N_{xy}\frac{\partial^2\omega}{\partial x\partial y}=0 \tag{10}$$

Substituting Eqs. (8) and (9) into Eq. (10), the stiffness of external plate can be obtained as Eq. (11).

$$D_r=\frac{bF_u}{k_{cr}\pi^2}-D_e \tag{11}$$

After the energy dissipation plate yield, the pots-yield stiffness is much smaller than the initial stiffness. Thus, the elastic buckling coefficient k_{cr} is not suitable for plastic buckling problem. Considering the plastic buckling of the energy dissipation plate, an elastic module reduction factor η is used. Bleich suggested an empirical equation for the elastic module reduction factor η, as shown in Eq. (12) [31]. Note that the units in Eq. (12) are 'N', 'MPa' and 'mm' for force, pressure, and length, respectively. Thus, the bending stiffness of the external plate D_r' can be derived as Eq. (13). The thickness t_r of the external restraining plate could be calculated as Eq. (14).

$$\eta=\frac{F_u(165-F_u/bt)^2}{5.93Etb} \tag{12}$$

$$D_r'=\frac{bF_u}{\sqrt{\eta}k_{cr}\pi^2}-D_e \tag{13}$$

$$t_r=\sqrt[3]{\frac{12D_r'\left(1-\nu^2\right)}{E}} \tag{14}$$

According to Eq. (14), the thickness of the BRSPD tested in the experiment study should be no less than 14.43 mm. The conclusion is consistent with the results obtained in the experiment study. S3 failed because of the inadequate thickness of the external restraining plate.

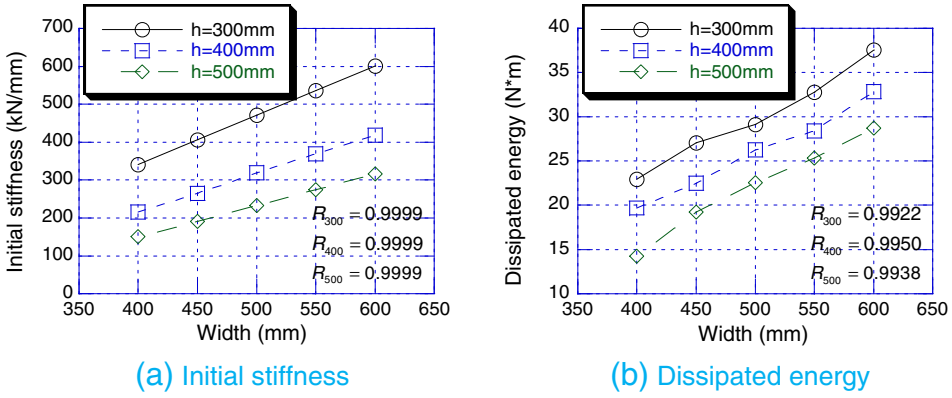

Fig. 12. Initial stiffness and energy dissipation capacity.

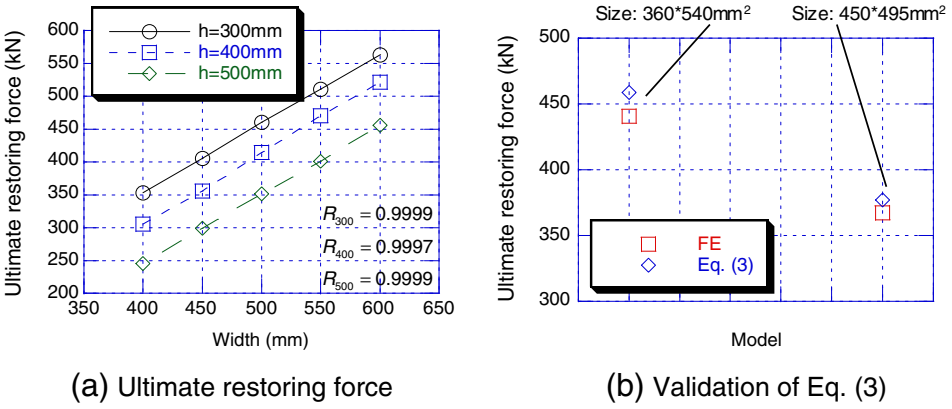

Fig. 13. Estimation of the ultimate restoring force.

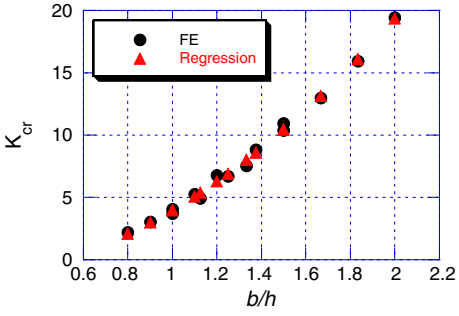

Fig. 14. Elastic buckling coefficient for the energy dissipation plate.

Two limitations should be noted for the application of Eq. (14), Firstly, the deformation compatibility, which was used in Eqs. (6) and (7), requires that the gaps between the energy dissipation plate and the external restraining plates are small enough. Otherwise the energy dissipation plate may have significant different out-of-plane deformation with the external restraining plate. Secondly, the size of the energy dissipation plate should not exceed the range of the models used in regression analysis for estimation of the ultimate restoring force F_u. Otherwise, Eq. (3) may lose its precision.

Two additional models, named A1 and A2, are built to validate the effectiveness of Eq. (14). These two models have the same energy dissipation plate with S1, but removing the stiffeners on the external restraining plates. The external restraining plates of A1 and A2 are 12-mm-thick and 20-mm-thick respectively. After 15 cycle loading at 1/20 shear deformation, the ultimate deformations of A1 and A2 are shown in Fig. 15. It can be observed that A1 has significant out-of-plane buckling. As for A2, the out-of-plane deformation is well restrained. The maximum out-of-plane deformations of A1 and A2 are 21.4 mm and 6.9 mm respectively, Furthermore, for A2, the maximum out-of-deformation occurred on the energy dissipation plate, demonstrating the effective restraint from 20-mm-thick restraining plate. Thus, Eq. (14) can be accepted.

In engineering practice, the stiffener on external restraining plate is recommended. As for S1 in the experimental study, based on the equation $I = ht_{eq}^3/12$, the equivalent thickness t_{eq} of the external restraining plate was 48.31 mm, which provides a much more reliable restraint to the energy dissipation plate.

6. Conclusions

A buckling restrained shear panel damper (BRSPD) is proposed in this study. Physical tests including five specimens were carried out to investigate the performance of the BRSPD. Numerical analyses were conducted to supplement the physical test results. Major conclusions obtained in this study are as follows:

1) Too large gaps between the external restraining plates and the energy dissipation plate lead to worse hysteresis performances of the BRSPD. Gaps not wider than 1 mm are recommended.
2) The equation for estimating the restoring force of the BRSPD was obtained based on the tests and analysis results. The ultimate restoring force of the BRSPD can be estimated using Eq. (3).
3) An appropriately designed external restraining plate can effectively restrain the out-of-plane buckling of the energy dissipation plate. The external restraining plate should be stiff enough to prevent the out-of-plane deformation of the external restraining plate. The stiffness of the external restraining plates should satisfy the requirement given in Eq. (13).

Acknowledgments

The authors gratefully acknowledge the financial support of the "Twelfth Five-Year Plan" major projects of the National Science and Technology under Grant No. 2012BAJ07B02 and the Natural Science Foundation of China under Grant No. 5117250.

References

[1] Tanaka K, Sasaki Y. Hysteretic performance of shear panel dampers of ultra-low-yield-strength steel for seismic response control of buildings [C]. 12th World Conference on Earthquake Engineering. New Zealand: WCEE; 2000.
[2] Pan P, Ye LP, Shi W, Shi W, Cao HY. Engineering practice of seismic isolation and energy dissipation structures in China [J]. Sci China Technol Sci 2012;55(11):3036–46.
[3] Soong TT, Spencer Jr BF. Supplemental energy dissipation: state-of-the-art and state-of-the-practice [J]. Eng Struct 2002;24(3):243–59.
[4] Chan RWK, Albermani F, Williams MS. Evaluation of yielding shear panel device for passive energy dissipation [J]. J Construct Steel Res 2009;65(2):260–8.
[5] Kurata N, Kobori T, Takahashi M, Niwa N. Study on active variable damping system for high-rise buildings in large earthquakes. Proceedings of the 1st European Conference on Structural Control, Barcelona; 1996. p. 402–9.
[6] Bosco M, Marino EM, Rossi PP. Proposal of modifications to the design provisions of Eurocode 8 for buildings with split k eccentric braces [J]. Eng Struct 2014;61(3):209–23.
[7] De Matteis G, Landolfo R, Mazzolani FM. Seismic response of MR steel frames with low-yield steel shear panels [J]. Eng Struct 2003;25(2):155–68.
[8] Nakashima M. Strain-hardening behavior of shear panels made of low-yield steel. I: test [J]. J Struct Eng 1995;121(12):1742–9.
[9] Nakashima M, Iwai S, Iwata M, Takeuchi T, Konomi S, Akazawa T, et al. Energy dissipation behaviour of shear panels made of low yield steel [J]. Earthquake Eng Struct Dyn 1994;23(12):1299–313.
[10] Rai DC, Annam PK, Pradhan T. Seismic testing of steel braced frames with aluminum shear yielding dampers [J]. Eng Struct 2013;46:737–47.
[11] De Matteis G, Brando G, Mazzolani FM. Hysteretic behaviour of bracing-type pure aluminium shear panels by experimental tests [J]. Earthquake Eng Struct Dyn 2011;40(10):1143–62.
[12] De Matteis G, Mazzolani FM, Panico S. Experimental tests on pure aluminium shear panels with welded stiffeners [J]. Eng Struct 2008;30(6):1734–44.
[13] Sahoo DR, Rai DC. Design and evaluation of seismic strengthening techniques for reinforced concrete frames with soft ground story [J]. Eng Struct 2013;56:1933–44.

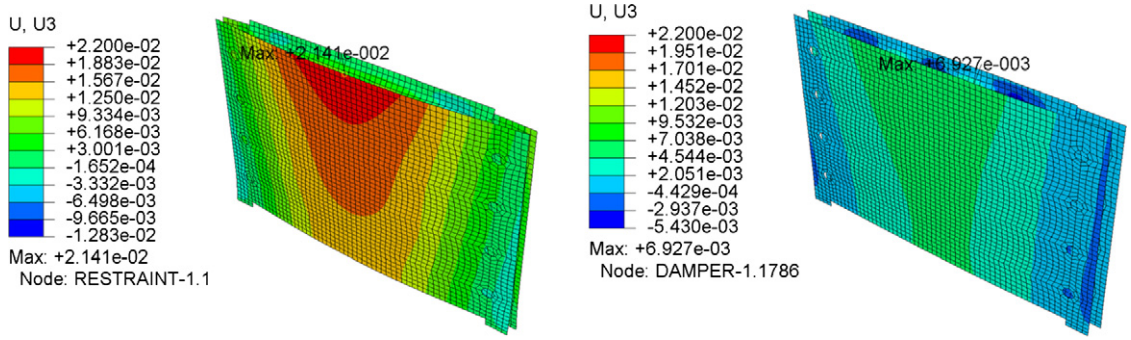

(a) A1 (12mm-thick restraining plate) (b) A2 (20mm-thick restraining plate)

Fig. 15. Ultimate deformation modes of A1 and A2.

[14] Brando G, De Matteis G. Design of low strength-high hardening metal multi-stiffened shear plates [J]. Eng Struct 2014;60:2–10.
[15] Ohsaki M, Nakajima T. Optimization of link member of eccentrically braced frames for maximum energy dissipation [J]. J Construct Steel Res 2012;75:38–44.
[16] Zhang C, Zhang Z, Shi J. Development of high deformation capacity low yield strength steel shear panel damper [J]. J Construct Steel Res 2012;75:116–30.
[17] Zhang C, Zhang Z, Zhang Q. Static and dynamic cyclic performance of a low-yield-strength steel shear panel damper [J]. J Construct Steel Res 2012;79:195–203.
[18] Fisher JW, Frank KH, Hirt MA, McNamee BM. Effect of weldments on the fatigue strength of steel beams. NCRP Report 102. Washington DC: Transportation Research Board; 1970.
[19] Engelhardt MD, Husain AS. Cyclic-loading performance of welded flange-bolted web connections [J]. J Struct Eng 1993;119(12):3537–50.
[20] Fatemi A, Yang L. Cumulative fatigue damage and life prediction theories: a survey of the state of the art for homogeneous materials [J]. Int J Fatigue 1998;20(1):9–34.
[21] Takahashi Y, Shinabe Y. Experimental study on restoring force characteristics of shear yielding thin steel plate elements [J]. J Struct Constr Eng 1997;494:107–14.
[22] Liu Y, Shimoda M. Shape optimization of shear panel damper for improving the deformation ability under cyclic loading [J]. Struct Multidisciplinary Opt 2013;1–9.
[23] Deng K, Pan P, Sun J, Liu J, Xue Y. Shape optimization design of steel shear panel dampers. J Constr Steel Res 2014;99(8):187–93.
[24] Brando G, D'Agostino F, De Matteis G. Experimental tests of a new hysteretic damper made of buckling inhibited shear panels [J]. Mater Struct 2013;46(12):2121–33.
[25] Ge H, Chen X, Matsui N. Seismic demand on shear panel dampers installed in steel-framed bridge pier structures [J]. J Earthquake Eng 2011;15(3):339–61.
[26] Ge HB, Kaneko K, Usami T. Capacity of stiffened steel shear panels as a structural control damper[C]. The 14th World Conference on Earthquake Engineering (14WCEE); 2008.
[27] Chinese Ministry of housing and urban rural development. Technical specification for seismic energy dissipation of buildings JGJ297-2013. China Architecture and Building Press; 2013.
[28] Shi Y, Wang M, Wang Y. Experimental and constitutive model study of structural steel under cyclic loading [J]. J Construct Steel Res 2011;67(8):1185–97.
[29] Dusicka P, Itani AM, Buckle IG. Cyclic response of plate steels under large inelastic strains [J]. J Construct Steel Res 2007;63(2):156–64.
[30] Timoshenko S, Woinowsky-Krieger S. Theory of plates and shells [M]. New York: McGraw-hill; 1959.
[31] Bleich F. Buckling strength of metal structures [M]. McGraw-Hill; 1952.